

Chemical Regeneration of Manganese Oxide-Coated Sand for Oxidation of Organic Stormwater Contaminants

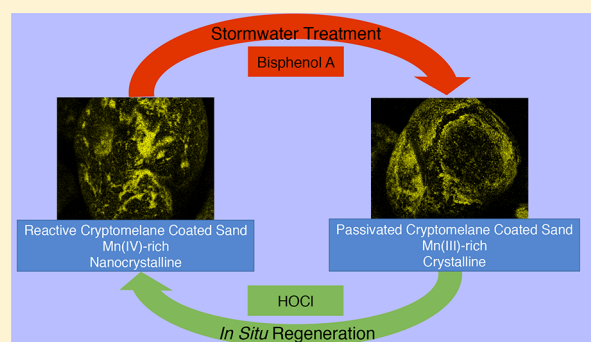
Joseph A. Charbonnet,[†] Yanghua Duan,[†] Case M. van Genuchten,[‡] and David L. Sedlak^{*,†}

[†]National Science Foundation Engineering Research Center for Reinventing the Nation's Urban Water Infrastructure (ReNUWIt) and Department of Civil & Environmental Engineering, University of California at Berkeley, Berkeley, California 94720, United States

[‡]Department of Earth Sciences, Geochemistry, Faculty of Geosciences, Utrecht University, Utrecht 3508TA, The Netherlands

Supporting Information

ABSTRACT: Urban stormwater, municipal wastewater effluent, and agricultural runoff contain trace amounts of organic contaminants that can compromise water quality. To provide a passive, low-cost means of oxidizing substituted phenols, aromatic amines, and other electron-rich organic compounds during infiltration of contaminated waters, we coated sand with manganese oxide using a new approach involving the room-temperature oxidation of Mn^{2+} with permanganate. Manganese oxide-coated sand effectively oxidized bisphenol A under typical infiltration conditions and sustained reactivity longer than previously described geomedia. Because geomedia reactivity decreased after extended operation, chlorine was evaluated for use as an in situ geomedia regenerant. Geomedia regenerated by HOCl demonstrated similar reactivity and longevity to that of virgin geomedia. Chemical analyses indicated that the average manganese oxidation state of the coatings decreased as the geomedia passivated. X-ray absorption spectroscopy and X-ray diffraction showed that the reactive virgin and regenerated geomedia coatings had nanocrystalline manganese oxide structures, whereas the failed geomedia coating exhibited greater crystallinity and resembled cryptomelane. These results suggest that it is possible to regenerate the oxidative capacity of manganese oxide-coated sands without excavating stormwater infiltration systems. These results also suggest that manganese oxide geomedia may be a cost-effective means of treating urban stormwater and other contaminated waters.



INTRODUCTION

Many water-stressed cities are considering investments in aquifer recharge projects in which urban stormwater, municipal wastewater effluent, or water from other potentially contaminated sources is intentionally percolated into a drinking water aquifer.^{1–3} This practice has the potential to contaminate groundwater with trace organic compounds.^{4,5} For example, urban stormwater contains low concentrations (i.e., typically less than 10 $\mu\text{g}/\text{L}$) of trace organic contaminants derived from asphalt, automobile wear and exhaust, biocides and consumer products that could be deleterious to human and ecosystem health.^{6–8} Municipal wastewater effluent contains organic compounds (e.g., pharmaceuticals, personal care products, and urban use pesticides) at similar concentrations.^{9,10}

During managed aquifer recharge, captured water is often percolated through gravel or sand.^{11,12} Manganese oxides are naturally occurring minerals that are capable of oxidizing many organic contaminants that contain electron-rich moieties, including substituted phenols, anilines, and thiols.^{13–15} Therefore, the introduction of manganese oxides as geomedia in an infiltration system could provide an inexpensive means of

treating organic contamination during the recharge process.^{16,17}

Bisphenol A is a contaminant of concern in stormwater and municipal wastewater effluent due to its potential impacts on the endocrine system.¹⁸ The reactions of bisphenol A with manganese oxides have been well-characterized.¹⁹ In the initial step of the transformation process, bisphenol A forms a surface complex with a $Mn(IV)$ –OH group which then undergoes a one-electron transfer, reducing $Mn(IV)$ sites to $Mn(III)$ and $Mn(III)$ sites to $Mn(II)$.^{14,20} The phenolate radical produced in the initial reaction can either diffuse away from the surface and react with other radicals to produce polymeric compounds or react again with the manganese oxide surface.^{21,22}

To exploit these reactions during managed aquifer recharge, manganese oxide-coated sand is preferable to pure manganese oxide minerals because of its higher hydraulic conductivity and lower propensity for advection from treatment systems.²³ After

Received: June 16, 2018

Revised: August 18, 2018

Accepted: August 20, 2018

Published: August 30, 2018

exposure to organic contaminants and other natural constituents (e.g., Ca^{2+} and NOM) the reactivity of manganese oxide-containing geomeedia decreases.²⁴ This passivation process appears to be related in part to the reduction of Mn(IV) sites and subsequent accumulation of Mn(II/III).^{17,25} Reoxidation of Mn(II) by atmospheric O_2 is unlikely to restore the reactivity of the geomeedia due to its slow kinetics under environmentally relevant conditions.²⁶ Biogenic production of a reactive manganese oxide phase (i.e., enzymatic catalysis of Mn[II] oxidation by O_2) is possible, but it would be difficult to implement and control in field applications.²⁷ It may be possible, however, to restore the reactivity of passivated geomeedia with a chemical oxidant. Such a process could facilitate the in situ regeneration of the manganese oxide-coated sand's reactivity, obviating the need for costly excavation and making the use of this engineered geomeedia less expensive and more practical.

The objective of this research was to develop a simple approach to produce and regenerate manganese oxide-coated sand that can be used as reactive geomeedia for oxidizing organic contaminants. By understanding the mechanisms and rates of the geomeedia passivation through spectroscopic and chemical analysis, it was possible to gain insight into approaches that could be used to prolong the useful lifetime of the geomeedia and regenerate its activity after failure.

MATERIALS AND METHODS

Reagents and Simulated Stormwater. All chemicals used in the synthesis and regeneration of manganese oxide-coated sand or for producing simulated stormwater were used as received from Fisher Chemical without further purification. A d-14 bisphenol A internal standard was obtained from Polymer Source, Inc. Ultrapure water was produced with a Milli-Q system ($R = 18.2 \text{ M}\Omega$) and was used for all dilutions and for geomeedia synthesis. All experiments were performed at room temperature.

Simulated stormwater was made as described by Grebel et al. (Table S1) which exhibited similar performance to that observed in authentic stormwater.²⁴ The simulated stormwater had $\text{pH } 7.0 \pm 0.1$, contained 1 mM total inorganic carbon, and had an ionic strength of 4.5 mM. Natural organic matter was not added to the simulated stormwater. Previous research indicated that natural organic matter concentrations typical of stormwater (i.e., 10 mg-C/L) result in only a modest decline in bisphenol A removal in both simulated and authentic stormwater.²⁴

Manganese Oxide-Coated Sand. Manganese oxide-coated sand was synthesized by modification of the cryptomelane synthesis method described by McKenzie,²⁸ which is similar to that reported by Lin et al.¹⁷ A total of 100 g of 20–30 mesh (595–841 μm) Fisher Ottawa sand was washed in 1 N nitric acid for 24 h. The sand was subsequently rinsed with Milli-Q water until the pH of the rinse effluent was above 6.0. After air drying, the sand was added to 250 mL of 2 N acetic acid containing 0.5 M MnSO_4 in a 1 L beaker. The sand was stirred vigorously with a magnetic stir bar as 200 mL of 0.43 M potassium permanganate solution was added dropwise over 30 min. The mixture was continuously stirred for an additional 90 min and allowed to settle overnight. After settling, the supernatant was decanted, and the coated sand was air-dried at 30 °C. The dry sand was sieved with 40 mesh and rinsed with Milli-Q water five times to remove loose manganese oxide and then redried prior to use in experiments.

When not in use, all geomeedia was stored in sealed amber glass bottles under N_2 at room temperature.

Geomeedia Longevity Tests. Glass columns with polyethylene fittings (16 mm inner diameter) were packed with 20 g of manganese oxide-coated sand to a height of 72 mm. Prior to packing, columns and tubing were sterilized by flushing with a 1% HCl solution followed by Milli-Q water. Columns were operated with saturated upward flow using a peristaltic pump and Tygon and PTFE tubing to deliver the simulated stormwater. Simulated stormwater containing 5 μM bisphenol A was pumped through the columns at 0.4 mL/min, equivalent to an infiltration rate of 9.5 cm/h. Geomeedia from one sacrificial replicate column was analyzed 98 h (approximately 500 pore volumes) into the longevity test. Column performance was monitored until the effluent bisphenol A exceeded 80% of influent concentration, at which point a plateau in performance occurred, and the geomeedia was deemed failed.²⁴ Failed geomeedia was rinsed with Milli-Q water for 2 h (10 pore volumes) to remove any residual organic compounds and then left in columns with ends capped for no more than 3 days.

Bisphenol A was quantified by an Agilent 6460 high performance liquid chromatography tandem-mass spectrometry (HPLC/MS-MS) system with electrospray ionization. Liquid chromatography was performed using an Agilent Zorbax SB-C18 column with 2.1 mm \times 50 mm dimensions and 3.5 μm pore size. 100 μL sample injection volumes were used with a mobile phase flow rate of 0.3 mL/min.

Total and dissolved manganese were measured with unfiltered and 0.22- μm syringe-filtered effluent samples, respectively. Samples were collected in plastic centrifuge tubes and immediately acidified before quantification by an Agilent 7700 Series Inductively Coupled Plasma-Mass Spectrometer (ICP-MS).

Geomeedia Regeneration. To determine the viability of in situ regeneration, failed geomeedia was left undisturbed following longevity tests and regenerated in columns. A solution of 0.31 mM HOCl buffered with 10 mM sodium acetate at pH 6 was applied at 0.4 mL/min over 50 h (i.e., five times stoichiometric demand of e^- equivalents required to oxidize the Mn[II/III] on the failed geomeedia to Mn[IV]). Geomeedia from one sacrificial replicate column was analyzed 10 h (50 pore volumes) into the longevity test, when stoichiometric demand was met. Regenerated geomeedia was rinsed with Milli-Q water for 2 h (10 pore volumes) after treatment to remove any residual regenerant and then left in the columns with ends capped for no more than 2 days. HOCl was quantified by the DPD method using a Shimadzu UV-2600 UV-vis spectrophotometer.²⁹

Geomeedia Characterization. The Mn coating density of the geomeedia was quantified by dissolving the manganese-oxide coating of a 0.5 g sample with 10 mL of 30 mM ascorbic acid and quantifying dissolved Mn by ICP-MS. Average Mn oxidation state was determined by the iodometric titration method.³⁰ Ion-exchangeable Mn was quantified by stirring 0.25 g of manganese oxide-coated sand in a 25 mL solution of 100 mM CaCl_2 overnight and then sampling through a 0.22 μm filter and quantifying Mn by ICP-MS.

X-ray diffraction (XRD) analysis was performed with a D8 Discover GADDS Powder XRD with a Fine-Focus Sealed Source ($\text{Cu K}\alpha$ radiation). To remove interference by the sand substrate, 3 g of sand was sonicated in 10 mL of acetone for 5 min to remove the coating. The suspended manganese oxide in

the supernatant was evaporatively deposited dropwise onto a zero-background SiO₂ sample holder.

Scanning electron microscopy was performed with a Zeiss EVO MA10 scanning electron microscope at 20 kV and a 1 nA current. Energy dispersive X-ray spectroscopy (EDS) was performed with a EDAX Genesis Imaging/Mapping analyzer.

Mn K-edge X-ray absorption spectroscopy (XAS) data were collected at beamline 4–1 of the Stanford Synchrotron Radiation Lightsources. Data were collected at liquid nitrogen temperature (77 K) in transmission and fluorescence modes out to a k value of 12.5 Å⁻¹. Transmission data were collected using ion chambers for measurements of I_0 and I_v while fluorescence data were collected using a PIPS detector. Due to the relatively low Mn concentration and the heterogeneous nature of the samples (Mn-rich coating, SiO₂ core), the fluorescence data were of superior quality and were thus used in data analysis. The monochromator was detuned 50% to prevent second-order harmonics, and the fluorescence data were collected using a PIPS detector. The vertical dimension of the X-ray beam during data collection was 2 mm, and the horizontal dimension was 10 mm. The XANES region was measured with 0.35 eV steps, whereas 0.05 Å⁻¹ steps were used for the EXAFS region. A total of 5 to 10 scans were collected for fluorescence measurements. A Mn(0) foil was used to calibrate the beam, with the maximum in the first derivative set to 6539 eV. Spectra were aligned, averaged, and background-subtracted using SixPack software following standard methods described previously.^{31,32} The EXAFS spectra were extracted using k^3 -weighting and were Fourier-transformed over the k -range 2–10 Å⁻¹ using a Kaiser-Bessel window with dk of 3 Å⁻¹. Samples were compared to the spectra of aqueous Mn(II), α -Mn₂O₃, and δ -MnO₂, obtained from a previous study.³¹ The XANES spectra of the samples were used to derive changes in Mn[II], Mn[III], and Mn[IV] content (Δ Mn[II], Δ Mn[III], and Δ Mn[IV]) from the virgin to the failed geomeia and from the failed to the regenerated geomeia. Because the fraction of Mn(II), Mn(III), and Mn(IV) derived from linear combination fits of the XANES spectra can vary depending on the selection of reference materials,³³ we performed four sets of linear combination fits using five reference materials with data from previously published papers^{31–35} on aqueous Mn(II), manganite, bixbyite, ramsdellite, and δ -MnO₂. The linear combination fits were performed with the SixPack software. For the linear combination fits, negative components were not allowed, and the sum of the components was not constrained to 1.0. We report the average and standard deviation of Δ Mn(II), Δ Mn(III), and Δ Mn(IV) values across the four linear combination fits, with the full linear combination fit output given (Table S3). This approach decreases errors in interpreting linear combination fit output due to the selection of particular reference materials.

RESULTS AND DISCUSSION

Geomeia Performance: Oxidation. After approximately 1300 pore volumes (i.e., 262 h) of exposure to a 5 μ M BPA solution of synthetic stormwater, the manganese oxide-coated sand failed (i.e., C/C_0 exceeded 0.80; Figure 1). Relative to the birnessite-coated sand with a similar Mn coating density tested by Grebel et al.,²⁴ which failed after approximately 250 pore volumes under identical conditions, this material exhibited exceptional performance. In addition, this manganese oxide-coated sand was produced at ambient temperatures, facilitating easier large-scale production than syntheses requiring high

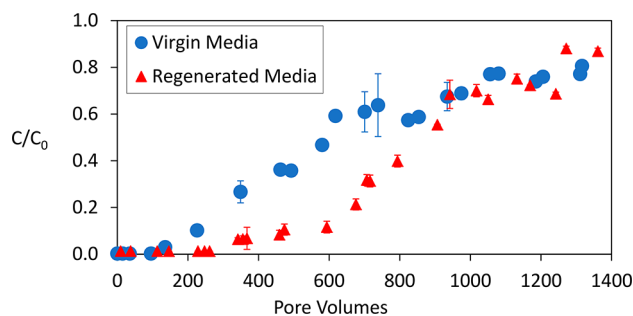


Figure 1. Concentration of bisphenol A leaving columns packed with 20 g of manganese oxide-coated sand. Longevity tests were conducted at a 0.4 mL/min flow rate with simulated stormwater containing 5 μ M bisphenol A. Geomeia was regenerated in situ at pH 6 with [HOCl] = 0.31 mM for 50 h. Error bars from triplicate samples are smaller than symbols in some cases.

reaction temperatures.^{28,36} Mineral properties, including surface area, reduction potential, and Mn oxidation state affect the reactivity of manganese oxide minerals.²² However, relatively few studies have demonstrated differences in the rate of oxidation of organic compounds by different manganese oxide minerals under well-controlled conditions.

10.6 of the 13.9 μ mol of influent bisphenol A were oxidized during the first 580 pore volumes of experimentation. 16.1 of the 31.4 μ mol of bisphenol A that entered the column during the entire 1300 pore volume experiment were oxidized. The reduction of manganese oxide implies that each transformed molecule of bisphenol A transferred an average of 21 electrons to manganese oxides in the column (see calculations; SI), which is consistent with previous reports that the initial products of bisphenol A oxidation also react with manganese oxides.²¹

The mass of Mn eluted from the columns due to reductive dissolution corresponded with the observed trends in bisphenol A oxidation. During the initial 40 min (3 pore volumes) of operation, Mn levels in the column effluent were above 80 μ M (inset in Figure 2), virtually all of which was

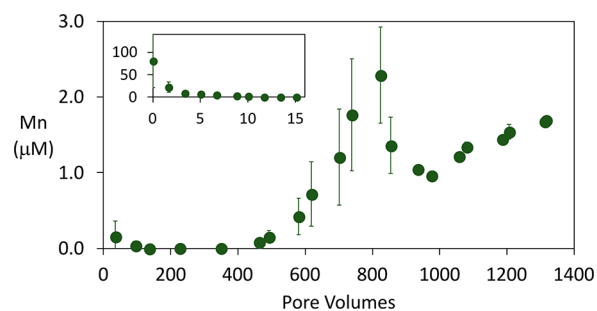


Figure 2. Total Mn leaving columns packed with 20 g of manganese oxide-coated sand. Inset shows the initial period of Mn release. Dissolved Mn concentrations were within 6% of total Mn for all time points. Error bars from triplicate samples are smaller than symbols in some cases.

dissolved. These data suggest there was an initial period of rapid Mn reduction to Mn²⁺, possibly due to a small proportion of highly reactive groups on the Mn-oxide surface. From 3 to 580 pore volumes, the geomeia removed more than half of influent bisphenol A yet effluent Mn concentrations remained below 0.5 μ M (Figure 2). This result was consistent with the reduction of Mn(IV) to Mn(III), which

would not produce high levels of soluble Mn. Between 580 and 975 pore volumes, effluent Mn concentrations increased, possibly due to the reduction of Mn(III) that was generated in the earlier stages of operation. After 975 pore volumes, effluent manganese decreased as the geomedia became less reactive. Approximately 6.4 mg of Mn (of a total of 40.2 g) was lost throughout the column operation period.

The release of Mn from geomedia is a water quality concern for aesthetic reasons.³⁷ Although effluent Mn concentrations exceeded the US EPA secondary standard for maximum total dissolved Mn of $0.91 \mu\text{M}$ ³⁸ near the start of the experiment, Mn release from this geomedia is not a major concern due to the relatively high concentration of the reactive compound giving rise to Mn(II) release (i.e., bisphenol A) and the likelihood of Mn(II) dilution, adsorption, and reoxidation as the water infiltrates the aquifer.

Geomedia Performance: Regeneration. The concentration of HOCl leaving the column during the regeneration process (Figure 3) increased from below $4 \mu\text{M}$ to over 0.21

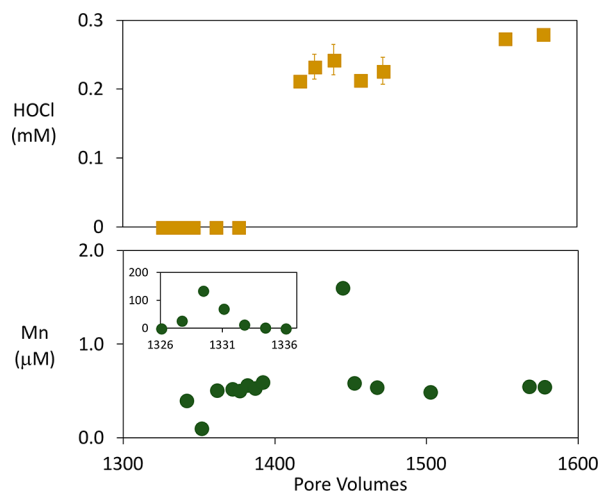


Figure 3. HOCl (top) and Mn (bottom) in effluent from column regeneration. 50-h regeneration with $[\text{HOCl}] = 0.31 \text{ mM}$ (5 times stoichiometric dose). HOCl concentrations below the $4 \mu\text{M}$ limit of detection are reported as 0. Mn in effluent during the initial phase of regeneration is inset. Regeneration experiments began after 1326 pore volumes had been passed through the columns.

mM after the theoretical chlorine demand was met (i.e., 1380 pore volumes into the experiment), suggesting the HOCl quickly oxidized the reduced Mn. During the initial 1.67 h (8 pore volumes) of regeneration up to $140 \mu\text{M}$ of dissolved Mn were detected in the water exiting the column. After this initial wash-out period, the effluent Mn concentration markedly decreased. However, during the 2-h rinse with Milli-Q water following regeneration, the Mn in the effluent increased to over $21 \mu\text{M}$, most of which was in the particulate phase.

Effluent manganese concentrations likely remained low for most of the regeneration period due to the oxidation of reduced Mn(II) and Mn(III) to Mn(IV) oxides by HOCl. The large release of manganese observed at the beginning of the regeneration period and during the rinse with Milli-Q water imply that manganese can be released following changes in influent composition between stormwater and oxidant solution. In particular, manganese oxide solids may slough off of the geomedia immediately following regeneration.

After regeneration, the manganese oxide-coated sand performed in a manner similar to that observed in the virgin geomedia (Figure 1). The regenerated geomedia initially removed all influent bisphenol A before failing after 1270 pore volumes (253 h). The regenerated geomedia sustained high reactivity with bisphenol A considerably longer than the virgin geomedia. Practically, these results suggest that regenerating manganese oxide-coated sand with HOCl could at least double its usable lifetime before failure due to the mechanism observed in this study.

Geomedia Characterization. The virgin manganese oxide-coated sand had a manganese coating density of $2.01 \pm 0.25 \text{ mg Mn/g geomedia}$ and an average Mn oxidation state of $+3.94 \pm 0.07$ (Figure 4) as measured by iodometric

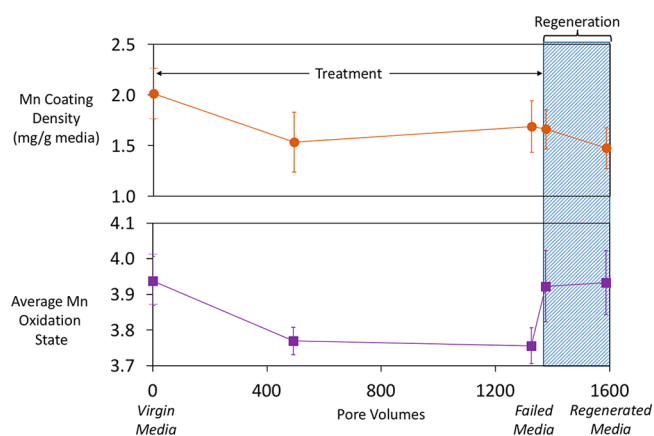


Figure 4. Evolution of Mn coating density of geomedia (top) and average Mn oxidation state (bottom) of geomedia in columns during longevity test (0–1326 pore volumes) and in situ regeneration (1326–1587 pore volumes) with HOCl. Virgin, failed, and regenerated geomedia are indicated below the *x*-axis.

titration. Likely due to initially rapid reduction of Mn, the coating density and oxidation state of manganese on the geomedia decreased over the first 500 pore volumes: the Mn coating density dropped to $1.53 \pm 0.18 \text{ mg Mn/g geomedia}$, while the average Mn oxidation state decreased to $+3.77 \pm 0.04$. The manganese coating density and the average oxidation state did not significantly change after these initial decreases. After approximately 1300 pore volumes, the failed manganese oxide-coated sand had a coating density of $1.69 \pm 0.26 \text{ mg Mn/g geomedia}$ and an average oxidation state of $+3.76 \pm 0.05$.

After regeneration at 5 times stoichiometric demand for 50 h, the manganese coating density was $1.47 \pm 0.20 \text{ mg Mn/g sand}$. Thus, over one test-regeneration cycle, 27% of the manganese in the geomedia was lost. Once stoichiometric oxidant demand was met (50 pore volumes into column regeneration), the average manganese oxidation state increased to $+3.92 \pm 0.1$. This value was not significantly changed by additional exposure to HOCl, suggesting the reduced manganese oxide was quickly oxidized to its final state by the HOCl and that a stoichiometric excess of oxidant was not necessary to restore the reactivity of the geomedia.

The geomedia was also characterized at different locations within the column, with each quartile (from most upstream to most downstream) analyzed separately after approximately 500 and 1300 pore volumes of longevity testing (Figure S1). After failure, the geomedia in the most upstream quartile had a

coating density of 1.55 ± 0.03 mg Mn/g sand, whereas the most downstream quartile of the column had a coating density of 1.95 ± 0.24 mg Mn/g sand. As expected, the coating density decreased more in the upstream portions of the column than in the downstream quartile, as reduced Mn dissolved. The reductive dissolution of Mn(IV/III) to Mn(II) was demonstrated by a decrease in Mn coating density in the upstream portions of the column and by the higher average oxidation state of the coating in the upstream portions of the column relative to the downstream portions.

Scanning electron microscopy images indicated no significant change in manganese oxide-coated sand morphology during the failure-regeneration cycle (Figure S2). Energy dispersive X-ray spectroscopy element mapping also showed similar extents of Mn coverage in all samples (Table S2).

The first derivative of the XANES spectrum of the failed sample (Figure S3) showed a subtle but systematic increase and decrease in amplitudes of the lower and higher energy shoulders in the main feature near 6547 and 6559 eV, respectively, relative to the virgin and regenerated samples. Based on the linear combination fits, the change in Mn(IV) content ($\Delta\text{Mn[IV]}$) from the virgin to the failed sample was $-8.3 \pm 2.2\%$, which was accompanied by a positive $\Delta\text{Mn(III)}$ of $+3.5 \pm 2.5\%$ (Table 1). The $\Delta\text{Mn(II)}$ between the virgin to

Table 1. Changes in Mn(II), Mn(III), and Mn(IV) Content Derived by LCFs

samples	$\Delta\text{Mn(II)}$	$\Delta\text{Mn(III)}$	$\Delta\text{Mn(IV)}$
virgin to failed geomeedia	$-0.1 \pm 0.1\%$	$+3.5 \pm 2.5\%$	$-8.3 \pm 2.2\%$
failed to regenerated geomeedia	$-0.7 \pm 0.8\%$	$-2.6 \pm 1.9\%$	$+7.0 \pm 1.4\%$

failed geomeedia was negligible (on average, the total solid phase Mn[II] for the virgin and failed geomeedia was <1%, Table S4). These results indicate a decrease in average Mn oxidation state in the failed material that was similar to that observed in the chemical titrations. The effectiveness of the HOCl regenerant in converting Mn(III) back to Mn(IV) was confirmed by the linear combination fits of the regenerated geomeedia, which showed a composition nearly identical to that of the virgin geomeedia, with $\Delta\text{Mn(IV)}$ from the failed to regenerated geomeedia of $+7.0 \pm 1.4\%$ and $\Delta\text{Mn(III)}$ of $-2.6 \pm 1.9\%$. Similar to the virgin material, the average Mn(II) content (and $\Delta\text{Mn[II]}$) for the regenerated geomeedia determined by linear combination fits was <1%, suggesting that the redox changes in the solid phase due to regeneration were dominantly due to cycling between Mn(III) and Mn(IV). The increase in Mn(III) abundance is consistent with the reduction of Mn(IV) to Mn(III) suggested by the low concentrations of soluble Mn observed in the column effluent between 20 and 580 pore volumes of column operation.

XRD patterns of the virgin and regenerated geomeedia coatings were similar, showing only broad peaks with low intensity at 12° , 28.8° , and 37.5° 2θ , which is indicative of nanocrystalline cryptomelane. The coating of the failed geomeedia exhibited intense peaks at $2\theta = 28.8^\circ$ ($d = 3.12$ Å) and 37.5° ($d = 2.40$ Å) that were considerably narrower than those observed in the virgin geomeedia. In addition, the failed material exhibited small, well-defined peaks (e.g., at 2θ near 42° and 48°) that were not apparent in the virgin geomeedia. These differences in the XRD patterns of the failed geomeedia relative to the virgin and regenerated material are consistent

with an increase in the crystallinity of the manganese oxide after it reacts with bisphenol A. The peak positions in the XRD patterns were consistent with monoclinic manganese oxide in the C12/m 1(12) space group (i.e., cryptomelane; Figure 5).³⁹

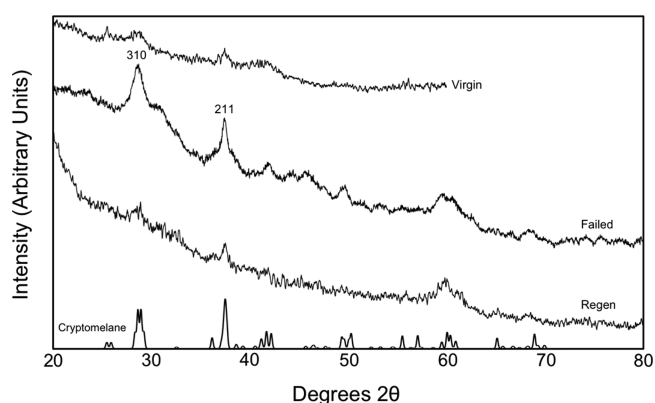


Figure 5. X-ray diffraction patterns for coating of virgin (top), failed (middle), and regenerated (bottom) manganese oxide-coated sand. The powder XRD pattern of cryptomelane (adapted from ref 39) is shown for comparison.

The Mn K-edge EXAFS spectra (Figure 6) of all geomeedia exhibited the staircase pattern from 4 to 6 \AA^{-1} characteristic of

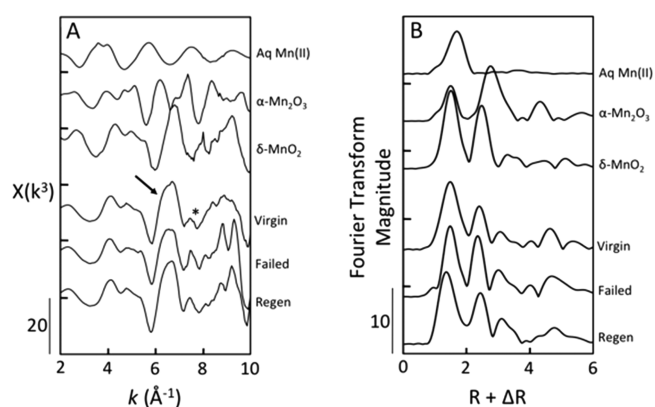


Figure 6. Mn K-edge EXAFS spectra (A) and Fourier transformed EXAFS spectra (B) of the virgin, failed, and regenerated (regen) manganese oxide-coated sand and standards of aqueous Mn(II), α -Mn₂O₃, and δ -MnO₂.

Mn(IV)-oxides. Additional features in the EXAFS spectra suggested a local coordination environment similar to cryptomelane,⁴⁰ particularly the humpbacked asymmetry of the oscillation at 6.8 \AA^{-1} (arrow in Figure 6), which is indicative of tunnel-structured MnO₆ octahedra.⁴¹ The more pronounced shoulder of this feature in the failed geomeedia suggests greater development of this structure.⁴¹ Subtle differences in the EXAFS spectra between the virgin, failed, and regenerated geomeedia were evident in the region from 7 to 8.5 \AA^{-1} (* symbol in Figure 6). This region in the EXAFS spectrum of the failed geomeedia exhibited a clearer double beat from 7 to 8.5 \AA^{-1} , which is another characteristic feature of tunnel-type Mn(IV) oxides, such as cryptomelane, todorokite, and psilomelane.⁴² The Fourier-transformed EXAFS spectra of all samples showed first- and second-shell peaks characteristic of the edge-sharing MnO₆ octahedra expected for Mn(IV) oxides (Figure 6). However, an additional peak at larger radial

distance, R , also appeared in all samples, which is characteristic of the corner-sharing MnO_6 octahedra that make up the tunnel structure of cryptomelane.^{31,41} Key differences between the virgin, failed, and regenerated geomedia appeared in the relative peak amplitudes of the Fourier transformed EXAFS spectra. The amplitude of the edge-sharing Mn–Mn peak relative to the Mn–O peak was largest in the failed geomedia, suggesting a more ordered Mn coordination environment in this sample. This result further suggests that the failed material was the most crystalline sample. This manganese oxide-coated sand, which was prepared using a modified cryptomelane synthesis method, may have demonstrated a longer reactive lifetime than birnessite-coated sands due to differences in reactivity between mineral forms of the manganese oxide or a higher average Mn oxidation state.²⁴ Birnessite has a layered structure and is frequently employed in experiments with organic compounds.^{13,24,43} In the cryptomelane structure, edge-sharing MnO_6 octahedra exhibit a tunnel-like, rather than sheet-like motif.⁴⁴ The difference in the arrangement of edge-sharing MnO_6 octahedra between these mineral polymorphs may explain the observed difference in their reactivity by exposing different crystal faces to solution.²²

Geomedia Passivation Mechanism. Results from the geomedia characterization provided evidence for the passivation mechanism wherein Mn(II) is initially released upon bisphenol A oxidation, followed by an increase in surface-associated Mn(III) and mineral crystallinity. The XRD and EXAFS spectra indicated that both the virgin and failed geomedia had nanocrystalline, cryptomelane-like coordination environments, while the failed geomedia coating was more crystalline. Additionally, chemical and XANES-derived oxidation state measurements demonstrate that Mn(III) was more abundant in the failed geomedia. However, very little Mn(II) was observed in any of the manganese oxide-coated sand.

In certain coordination environments, particularly at edge sites, Mn(III/IV) groups can be highly reactive.^{45–48} The initial removal of greater than 98% of bisphenol A in the columns (i.e., before 150 pore volumes), coupled with the release of considerable amounts of Mn(II) may have been due to the reduction of these highly reactive sites.

The relatively fast geomedia passivation between 150 and 580 pore volumes was consistent with the reduction of Mn(IV) to less-reactive structural Mn(III) sites.⁴⁹ The increased crystallinity and simultaneous decrease in oxidation state are significant because less crystalline manganese oxides typically have higher concentrations of reactive sites and are more reactive than their crystalline counterparts.^{31,50,51} This crystallization may be particularly important to cryptomelane. A mineral consisting of a network of tunnels may have a lower surface area accessible to dissolved organic species in the bulk solution upon crystallization, causing a more pronounced decrease in reactivity with crystal growth than might occur with phyllophanates, if the organic molecule is too large to access tunnel sites. From 580 to 975 pore volumes, the sustained removal of 30–40% of influent bisphenol A demonstrates that the Mn(III)-rich cryptomelane retained some reactivity. The reductive dissolution of the Mn(III) was consistent with the increase of Mn(II) in the column effluent at later stages of the experiment and the negligible change in average Mn oxidation state as bisphenol A was oxidized and reduced Mn was released from the surface.

Mn^{2+} produced by the reaction can passivate manganese oxide-coated sand by blocking reactive sites.^{52,53} However,

given the small amount of Mn(II) detected in the geomedia, we conclude that Mn^{2+} contributed little to the observed passivation.

Several researchers have reported that manganese oxides adsorb bisphenol A as a precursor to oxidation and that reversible sorption is unimportant compared to oxidation.^{21,24,25} After passing Milli-Q water through the failed columns for 10 pore volumes, the concentration of bisphenol A coming out of the columns was $0.9 \mu\text{M}$, which was approximately equal to the concentration observed in control columns filled with acid-washed sand under identical conditions. The small mass of bisphenol A ($9.9 \mu\text{g}$, 0.14% of the total influent) released during the rinse step was likely associated with the short sections of polyethylene fittings and Tygon tubing in the columns and peristaltic pumps. The major transformation products of bisphenol A, including 4-hydroxycumyl alcohol, do not reversibly sorb to manganese oxides in appreciable amounts under the conditions employed in these experiments.^{13,19} Therefore, it is unlikely that adsorbed bisphenol A or its transformation products contributed significantly to the passivation of the geomedia.

Microbial activity may have influenced the trend of geomedia performance. Although columns and tubing were sterilized with 1% HCl before testing, the possibility of inducing phase change or chemical transformation reactions made chemical or thermal sterilization of manganese oxide-coated sand or bisphenol A stocks infeasible. Bisphenol A may have been biotransformed or absorbed by biofilms after several weeks of longevity testing, resulting in higher apparent reactivity and slower passivation of the geomedia.⁵⁴ Because the concentration of bisphenol A observed after column failure was approximately equal to the inlet concentration, (i.e., $[C]/[C_0] > 0.8$) and there is no reason to expect that microbial activity would suddenly cease after 1000 pore volumes, we conclude that losses by this mechanism were unimportant relative to reactions with the Mn-oxide coated sands.

Regeneration Mechanism. The virgin and regenerated geomedia had comparable reactivity and longevity and similar XRD and XAS spectra that suggest that both geomedia types were coated with poorly ordered cryptomelane phases. This finding implies that the local coordination environment of the manganese oxide was largely preserved after regeneration (i.e., cryptomelane remained the dominant phase), but the disorder increased as the average Mn oxidation state rose.

Treatment with HOCl can oxidize surface-associated Mn(III), including those in crystal lattice orientations that may have played a role in decreasing surface reactivity.⁵⁵ The rapid reoxidation of the passivated manganese and the efficient scavenging of HOCl suggest that the oxidation of Mn(III) occurred quickly during regeneration. It may be possible that the oxidation of Mn(III) to Mn(IV) resulted in the loss of Jahn–Teller distortion, producing strain in the mineral, resulting in some bonds breaking and smaller crystal size. This process may have generated a mineral phase that, in addition to being more oxidized, was less ordered and more reactive with organic compounds. Unfortunately, the oxidation of Mn(III)-rich oxides has not been studied as extensively as Mn^{2+} oxidation.^{31,56,57} Determination of the mechanisms of surface-associated Mn(III) oxidation could provide more insight into the nature of the manganese oxide generated in the reaction and the local structure of reactive sites.

ENVIRONMENTAL IMPLICATIONS

Given its superior performance and relative ease of production, the manganese oxide-coated sand used in this study shows considerable promise for field applications. For example, a typical-sized stormwater infiltration system that treats 2×10^6 L of stormwater per year may cover 50 m² of ground surface with a 0.5 m-deep layer of manganese oxide-coated sand.⁵⁸ Assuming stormwater containing 50 µg/L of natural and anthropogenic oxidizable organic compounds, such a system could be expected to operate for decades before loss of reactivity occurs due to the mechanism observed in this study. Without regeneration, the system could operate approximately 45 years before a 20% loss of reactivity, 80 years before a 50% loss of reactivity, and 175 years before an 80% loss of reactivity (see calculations; SI). Although approximately 25% of the Mn coating density of the geomedia was lost during one cycle of treatment and regeneration, the observation that manganese oxide reactivity did not change over the two treatment-regeneration cycles tested and the rates of Mn coating loss suggest that this geomedia would be effective for multiple treatment-regeneration cycles under field conditions. If the Mn coating density decreases substantially after several treatment-regeneration cycles, more frequent geomedia regeneration may be required. It is possible that other processes, including clogging by suspended solids and microbial growth, could cause more rapid failure in field applications of this technology than were observed in this laboratory study.⁵⁹ Researchers studying field-scale systems have employed settling prior to infiltration and bioturbation by plant roots as effective countermeasures to clogging.^{6,60} The successful application of biogenic manganese oxides as a polishing step for municipal wastewater effluent suggests that, while biological activity can slow reactions, it will not necessarily adversely affect the reactivity of manganese oxides.⁶¹

Manganese oxide geomedia are only capable of oxidizing certain organic stormwater contaminants.²⁴ Therefore, other geomedia, such as biochar, would be needed if runoff containing contaminants that do not react with the manganese oxide.⁶² Prior research suggests that oxidation of the bisphenol A by manganese oxide coated-sand produces 4-hydroxycumyl alcohol,²⁴ which is more estrogenic than its parent compound.⁶³ 4-Hydroxycumyl alcohol is susceptible to further biotransformation under oxic environments such as those encountered in stormwater infiltration systems.²¹ Oxidation by manganese oxides does not always result in the mineralization, and therefore complete detoxification, of contaminants. However, the products of partial oxidation are frequently more susceptible to biotransformation or removal as they encounter other geomedia (e.g., biochar) deployed alongside manganese oxide-coated sand.^{6,19} Organic compounds with electron-withdrawing moieties are slow to react with manganese oxide-coated sand.²⁴ Nonetheless, the oxidation of organic contaminants by manganese oxides frequently diminishes the endocrine disrupting potential of the product water.^{64,65}

The introduction of hypochlorite to the subsurface during the regeneration process could result in the production of chlorine disinfection byproducts.⁶⁶ Because the reduced Mn reacted with HOCl very efficiently, proper dosing during regeneration would limit the formation of disinfection byproducts. Furthermore, if the chlorine solution used for regeneration consists of potable water, many of the disinfection

byproduct precursors would likely have been removed.⁶⁷ To minimize the potential for introducing these disinfection byproducts into the groundwater during regeneration, stormwater infiltration systems could be hydraulically isolated, allowing for the effluent from the regeneration process to be collected and disposed of rather than undergoing infiltration.⁶⁸ Regeneration of a 50 m² treatment system would require approximately 228 m³ of a 25 mg HOCl-Cl₂/L solution (see calculations; SI). This corresponds to approximately 200 L of a 3% solution of NaOCl (i.e., household bleach) which could be handled by a field crew without the need for extraordinary precautions.

This study provides insights into how subtle changes in manganese oxide oxidation state and mineralogy can have large implications for reactivity. Although the cryptomelane coating in this study has a slightly higher average manganese oxidation state than is usually found in naturally occurring cryptomelane,⁶⁹ these results suggest that cryptomelane may be an important manganese oxide species given its relevance in both natural and engineered environments.⁷⁰ Cryptomelane is less frequently studied than birnessite and may have differences in reactivity and weathering due to its distinct structure.⁴⁰ This study begins to elucidate mineralogy–reactivity relationships and how manganese oxide structure transforms during redox reactions.

Although this study focused on stormwater infiltration applications, this geomedia may have other applications, including managed aquifer recharge with municipal wastewater effluent and agricultural runoff.^{11,71} Manganese oxides may also have applications in advanced wastewater treatment.^{61,64,72} Manganese and iron oxide-coated sand are already frequently used to remove dissolved metals during drinking water treatment.^{73–75} The methods described here may lead to geomedia with a longer lifetime that is less expensive to utilize and regenerate.

ASSOCIATED CONTENT

Supporting Information

The Supporting Information is available free of charge on the ACS Publications website at DOI: 10.1021/acs.est.8b03304.

Details of simulated stormwater composition, changes in geomedia coating (inc. SEM/EDS images), XANES spectra and linear combination fits, and estimation of geomedia lifetime (PDF)

AUTHOR INFORMATION

Corresponding Author

*Phone: (510)643-0256; e-mail: sedlak@berkeley.edu.

ORCID

Joseph A. Charbonnet: 0000-0001-8766-6072

David L. Sedlak: 0000-0003-1686-8464

Notes

The authors declare no competing financial interest.

ACKNOWLEDGMENTS

This research was supported by the National Science Foundation (NSF) through the Engineering Research Center for Re-Inventing the Nation's Water Infrastructure (ReNU-WIt) EEC-1028968. This material is also based upon work supported by the National Science Foundation Graduate Research Fellowship under Grant No. DGE 1106400 and

NWO Veni Grant (Project No. 14400). Use of the Stanford Synchrotron Radiation Lightsource, SLAC National Accelerator Laboratory, is supported by the U.S. Department of Energy, Office of Science, Office of Basic Energy Sciences under Contract No. DE-AC02-76SF00515.

REFERENCES

- (1) Page, D.; Miotliński, K.; Gonzalez, D.; Barry, K.; Dillon, P.; Gallen, C. Environmental Monitoring of Selected Pesticides and Organic Chemicals in Urban Stormwater Recycling Systems Using Passive Sampling Techniques. *J. Contam. Hydrol.* **2014**, *158*, 65–77.
- (2) Daigger, G. T. Evolving Urban Water and Residuals Management Paradigms: Water Reclamation and Reuse, Decentralization, and Resource Recovery. *Water Environ. Res.* **2009**, *81* (8), 809–823.
- (3) Bradshaw, J. L.; Luthy, R. G. Modeling and Optimization of Recycled Water Systems to Augment Urban Groundwater Recharge through Underutilized Stormwater Spreading Basins. *Environ. Sci. Technol.* **2017**, *51* (20), 11809–11819.
- (4) Page, D.; Dillon, P.; Vanderzalm, J.; Toze, S.; Sidhu, J.; Barry, K.; Levett, K.; Kremer, S.; Regel, R. Risk Assessment of Aquifer Storage Transfer and Recovery with Urban Stormwater for Producing Water of a Potable Quality. *J. Environ. Qual.* **2010**, *39* (6), 2029–2039.
- (5) Andres, A. S.; Ballester, T. P.; Musick, M. L. Stormwater Management: When Is Green Not So Green? *Groundwater* **2018**, *56* (3), 357–358.
- (6) Grebel, J. E.; Mohanty, S. K.; Torkelson, A. A.; Boehm, A. B.; Higgins, C. P.; Maxwell, R. M.; Nelson, K. L.; Sedlak, D. L. Engineered Infiltration Systems for Urban Stormwater Reclamation. *Environ. Eng. Sci.* **2013**, *30* (8), 437–454.
- (7) Makepeace, D. K.; Smith, D. W.; Stanley, S. J. Urban Stormwater Quality: Summary of Contaminant Data. *Crit. Rev. Environ. Sci. Technol.* **1995**, *25* (2), 93–139.
- (8) Jasper, J. T.; Nguyen, M. T.; Jones, Z. L.; Ismail, N. S.; Sedlak, D. L.; Sharp, J. O.; Luthy, R. G.; Horne, A. J.; Nelson, K. L. Unit Process Wetlands for Removal of Trace Organic Contaminants and Pathogens from Municipal Wastewater Effluents. *Environ. Eng. Sci.* **2013**, *30* (8), 421–436.
- (9) Bolong, N.; Ismail, A. F.; Salim, M. R.; Matsuura, T. A Review of the Effects of Emerging Contaminants in Wastewater and Options for Their Removal. *Desalination* **2009**, *239* (1–3), 229–246.
- (10) Clara, M.; Strenn, B.; Gans, O.; Martinez, E.; Kreuzinger, N.; Kroiss, H. Removal of Selected Pharmaceuticals, Fragrances and Endocrine Disrupting Compounds in a Membrane Bioreactor and Conventional Wastewater Treatment Plants. *Water Res.* **2005**, *39* (19), 4797–4807.
- (11) Dillon, P.; Pavelic, P.; Page, D.; Beringen, H.; Ward, J. *Managed Aquifer Recharge: An Introduction*; Australia National Water Commission: Canberra, A.C.T., 2009.
- (12) Pitt, R.; Talebi, L.; Bean, R.; Clark, S. *Stormwater Non-Potable Beneficial Uses and Effects on Urban Infrastructure*; Water Environment Research Foundation: Alexandria, VA, 2012.
- (13) Lin, K.; Liu, W.; Gan, J. Oxidative Removal of Bisphenol A by Manganese Dioxide: Efficacy, Products, and Pathways. *Environ. Sci. Technol.* **2009**, *43* (10), 3860–3864.
- (14) Stone, A. T. Reductive Dissolution of Manganese (III/IV) Oxides by Substituted Phenols. *Environ. Sci. Technol.* **1987**, *21* (10), 979–988.
- (15) Laha, S.; Luthy, R. G. Oxidation of Aniline and Other Primary Aromatic Amines by Manganese Dioxide. *Environ. Sci. Technol.* **1990**, *24* (3), 363–373.
- (16) Hatt, B. E.; Fletcher, T. D.; Deletic, A. Hydraulic and Pollutant Removal Performance of Fine Media Stormwater Filtration Systems. *Environ. Sci. Technol.* **2008**, *42* (7), 2535–2541.
- (17) Lin, K.; Peng, Y.; Huang, X.; Ding, J. Transformation of Bisphenol A by Manganese Oxide-Coated Sand. *Environ. Sci. Pollut. Res.* **2013**, *20* (3), 1461–1467.
- (18) Vandenberg, L. N.; Hauser, R.; Marcus, M.; Olea, N.; Welshons, W. V. Human Exposure to Bisphenol A (BPA). *Reprod. Toxicol.* **2007**, *24* (2), 139–177.
- (19) Im, J.; Löffler, F. E. Fate of Bisphenol A in Terrestrial and Aquatic Environments. *Environ. Sci. Technol.* **2016**, *50* (16), 8403–8416.
- (20) Zhang, H.; Chen, W.-R.; Huang, C.-H. Kinetic Modeling of Oxidation of Antibacterial Agents by Manganese Oxide. *Environ. Sci. Technol.* **2008**, *42* (15), 5548–5554.
- (21) Im, J.; Prevatte, C. W.; Campagna, S. R.; Löffler, F. E. Identification of 4-Hydroxycumyl Alcohol As the Major MnO₂-Mediated Bisphenol A Transformation Product and Evaluation of Its Environmental Fate. *Environ. Sci. Technol.* **2015**, *49* (10), 6214–6221.
- (22) Remucal, C. K.; Ginder-Vogel, M. A Critical Review of the Reactivity of Manganese Oxides with Organic Contaminants. *Environ. Sci. Process. Impacts* **2014**, *16* (6), 1247–1266.
- (23) Liu, D.; Sansalone, J. J.; Cartledge, F. K. Comparison of Sorptive Filter Media for Treatment of Metals in Runoff. *J. Environ. Eng.* **2005**, *131* (8), 1178–1186.
- (24) Grebel, J. E.; Charbonnet, J. A.; Sedlak, D. L. Oxidation of Organic Contaminants by Manganese Oxide Geomedia for Passive Urban Stormwater Treatment Systems. *Water Res.* **2016**, *88*, 481–491.
- (25) Balgooyen, S.; Alaimo, P. J.; Remucal, C. K.; Ginder-Vogel, M. Structural Transformation of MnO₂ during the Oxidation of Bisphenol A. *Environ. Sci. Technol.* **2017**, *51* (11), 6053–6062.
- (26) Von Langen, P. J.; Johnson, K. S.; Coale, K. H.; Elrod, V. A. Oxidation Kinetics of Manganese (II) in Seawater at Nanomolar Concentrations. *Geochim. Cosmochim. Acta* **1997**, *61* (23), 4945–4954.
- (27) Learman, D. R.; Wankel, S. D.; Webb, S. M.; Martinez, N.; Madden, A. S.; Hansel, C. M. Coupled Biotic–Abiotic Mn(II) Oxidation Pathway Mediates the Formation and Structural Evolution of Biogenic Mn Oxides. *Geochim. Cosmochim. Acta* **2011**, *75* (20), 6048–6063.
- (28) McKenzie, R. M. The Synthesis of Birnessite, Cryptomelane, and Some Other Oxides and Hydroxides of Manganese. *Mineral. Mag.* **1971**, *38* (296), 493–502.
- (29) Moberg, L.; Karlberg, B. An Improved N, N'-Diethyl-p-Phenylenediamine (DPD) Method for the Determination of Free Chlorine Based on Multiple Wavelength Detection. *Anal. Chim. Acta* **2000**, *407* (1), 127–133.
- (30) Murray, J. W.; Balistrieri, L.; Paul, B. The Oxidation State of Manganese in Marine Sediments and Ferromanganese Nodules. *Geochim. Cosmochim. Acta* **1984**, *48*, 1237–1247.
- (31) van Genuchten, C. M.; Peña, J. Mn(II) Oxidation in Fenton and Fenton Type Systems: Identification of Reaction Efficiency and Reaction Products. *Environ. Sci. Technol.* **2017**, *51* (5), 2982–2991.
- (32) Webb, S. M. SIXPack a Graphical User Interface for XAS Analysis Using IFEFFIT. *Phys. Scr.* **2005**, *1011*, 1011–1014.
- (33) Manceau, A.; Marcus, M. A.; Grangeon, S. Determination of Mn Valence States in Mixed-Valent Manganates by XANES Spectroscopy. *Am. Mineral.* **2012**, *97* (5–6), 816–827.
- (34) Marafatto, F. F.; Strader, M. L.; Gonzalez-Holguera, J.; Schwartzberg, A.; Gilbert, B.; Peña, J. Rate and Mechanism of the Photoreduction of Birnessite (MnO₂) Nanosheets. *Proc. Natl. Acad. Sci. U. S. A.* **2015**, *112* (15), 4600–4605.
- (35) Webb, S. M. SIXPack a Graphical User Interface for XAS Analysis Using IFEFFIT. *Phys. Scr.* **2005**, *1011*, 1011–1014.
- (36) McKenzie, R. M. The Reaction of Cobalt with Manganese Dioxide Minerals. *Aust. J. Soil Res.* **1970**, *8* (1), 97–106.
- (37) Sain, A. E.; Dietrich, A. M. Rethinking Aesthetic Guidelines for Manganese and Iron in Drinking Water. *Aqua* **2015**, *64* (7), 775–782.
- (38) US Environmental Protection Agency *National Recommended Water Quality Criteria*; Office of Science and Technology: Office of Water: Washington, DC, 2004.
- (39) Post, J. E.; von Dreele, R. B.; Buseck, P. R. Symmetry and Cation Displacements in Hollandites: Structure Refinements of

Hollandite, Cryptomelane and Priderite. *Acta Crystallogr., Sect. B: Struct. Crystallogr. Cryst. Chem.* **1982**, *38*, 1056–1065.

(40) Kim, S. S.; Bargar, J. R.; Nealson, K. H.; Flood, B. E.; Kirschvink, J. L.; Raub, T. D.; Tebo, B. M.; Villalobos, M. Searching for Biosignatures Using Electron Paramagnetic Resonance (EPR) Analysis of Manganese Oxides. *Astrobiology* **2011**, *11* (8), 775–786.

(41) Manceau, A.; Combes, J. M. Structure of Mn and Fe Oxides and Oxyhydroxides: A Topological Approach by EXAFS. *Phys. Chem. Miner.* **1988**, *15* (3), 283–295.

(42) Manceau, A.; Kersten, M.; Marcus, M. A.; Geoffroy, N.; Granina, L. Ba and Ni Speciation in a Nodule of Binary Mn Oxide Phase Composition from Lake Baikal. *Geochim. Cosmochim. Acta* **2007**, *71* (8), 1967–1981.

(43) Zhang, H.; Huang, C.-H. Oxidative Transformation of Triclosan and Chlorophene by Manganese Oxides. *Environ. Sci. Technol.* **2003**, *37* (11), 2421–2430.

(44) Robinson, D. M.; Go, Y. B.; Mui, M.; Gardner, G.; Zhang, Z.; Mastrogiovanni, D.; Garfunkel, E.; Li, J.; Greenblatt, M.; Dismukes, G. C. Photochemical Water Oxidation by Crystalline Polymorphs of Manganese Oxides: Structural Requirements for Catalysis. *J. Am. Chem. Soc.* **2013**, *135* (9), 3494–3501.

(45) Simanova, A. A.; Peña, J. Time-Resolved Investigation of Cobalt Oxidation by Mn(III)-Rich δ -MnO₂ Using Quick X-Ray Absorption Spectroscopy. *Environ. Sci. Technol.* **2015**, *49* (18), 10867–10876.

(46) Nico, P. S.; Zasoski, R. J. Mn(III) Center Availability as a Rate Controlling Factor in the Oxidation of Phenol and Sulfide on δ -MnO₂. *Environ. Sci. Technol.* **2001**, *35* (16), 3338–3343.

(47) Manceau, A.; Drits, V. A.; Silvester, E.; Bartoli, C.; Lanson, B. Structural Mechanism of Co²⁺ Oxidation by the Phyllosilicate Buserite. *Am. Mineral.* **1997**, *82*, 1150–1175.

(48) Liu, C. S.; Zhang, L. J.; Feng, C. H.; Wu, C. A.; Li, F. B.; Li, X. Z. Relationship between Oxidative Degradation of 2-Mercaptobenzothiazole and Physicochemical Properties of Manganese (Hydro)-Oxides. *Environ. Chem.* **2009**, *6* (1), 83.

(49) Liu, C.; Zhang, L.; Li, F.; Wang, Y.; Gao, Y.; Li, X.; Cao, W.; Feng, C.; Dong, J.; Sun, L. Dependence of Sulfadiazine Oxidative Degradation on Physicochemical Properties of Manganese Dioxides. *Ind. Eng. Chem. Res.* **2009**, *48* (23), 10408–10413.

(50) Hou, J.; Li, Y.; Mao, M.; Ren, L.; Zhao, X. Tremendous Effect of the Morphology of Birnessite-Type Manganese Oxide Nanostructures on Catalytic Activity. *ACS Appl. Mater. Interfaces* **2014**, *6* (17), 14981–14987.

(51) Villalobos, M.; Carrillo-Cárdenas, M.; Gibson, R.; López-Santiago, N. R.; Morales, J. A. The Influence of Particle Size and Structure on the Sorption and Oxidation Behaviour of Birnessite: II. Adsorption and Oxidation of Four Polycyclic Aromatic Hydrocarbons. *Environ. Chem.* **2014**, *11* (3), 279–288.

(52) Gao, N.; Hong, J.; Yu, Z.; Peng, P.; Huang, W. Transformation of Bisphenol A in the Presence of Manganese Dioxide. *Soil Sci.* **2011**, *176* (6), 265–272.

(53) Klausen, J.; Haderlein, S. B.; Schwarzenbach, R. P. Oxidation of Substituted Anilines by Aqueous MnO₂: Effect of Co-Solutes on Initial and Quasi-Steady-State Kinetics. *Environ. Sci. Technol.* **1997**, *31* (9), 2642–2649.

(54) Kang, J.-H.; Kondo, F. Bisphenol A Degradation by Bacteria Isolated from River Water. *Arch. Environ. Contam. Toxicol.* **2002**, *43* (3), 265–269.

(55) Elzinga, E. J. ⁵⁴Mn Radiotracers Demonstrate Continuous Dissolution and Re-precipitation of Vernadite (δ -MnO₂) during Interaction with Aqueous Mn(II). *Environ. Sci. Technol.* **2016**, *50* (16), 8670–8677.

(56) Webb, S. M.; Dick, G. J.; Bargar, J. R.; Tebo, B. M. Evidence for the Presence of Mn (III) Intermediates in the Bacterial Oxidation of Mn (II). *Proc. Natl. Acad. Sci. U. S. A.* **2005**, *102* (15), 5558–5563.

(57) Nico, P. S.; Zasoski, R. J. Importance of Mn(III) Availability on the Rate of Cr(III) Oxidation on δ -MnO₂. *Environ. Sci. Technol.* **2000**, *34* (16), 3363–3367.

(58) Hatt, B. E.; Fletcher, T. D.; Deletic, A. Pollutant Removal Performance of Field-Scale Stormwater Biofiltration Systems. *Water Sci. Technol.* **2009**, *59* (8), 1567.

(59) Alidina, M.; Li, D.; Ouf, M.; Drewes, J. E. Role of Primary Substrate Composition and Concentration on Attenuation of Trace Organic Chemicals in Managed Aquifer Recharge Systems. *J. Environ. Manage.* **2014**, *144*, 58–66.

(60) Le Coustumer, S.; Fletcher, T. D.; Deletic, A.; Barraud, S.; Poelsma, P. The Influence of Design Parameters on Clogging of Stormwater Biofilters: A Large-Scale Column Study. *Water Res.* **2012**, *46* (20), 6743–6752.

(61) Forrez, I.; Carballa, M.; Verbeken, K.; Vanhaecke, L.; Ternes, T.; Boon, N.; Verstraete, W. Diclofenac Oxidation by Biogenic Manganese Oxides. *Environ. Sci. Technol.* **2010**, *44* (9), 3449–3454.

(62) Ulrich, B. A.; Loehnert, M.; Higgins, C. P. Improved Contaminant Removal in Vegetated Stormwater Biofilters Amended with Biochar. *Environ. Sci. Water Res. Technol.* **2017**, *3* (4), 726–734.

(63) Nakamura, S.; Tezuka, Y.; Ushiyama, A.; Kawashima, C.; Kitagawara, Y.; Takahashi, K.; Ohta, S.; Mashino, T. Ipso Substitution of Bisphenol A Catalyzed by Microsomal Cytochrome P450 and Enhancement of Estrogenic Activity. *Toxicol. Lett.* **2011**, *203* (1), 92–95.

(64) Forrez, I.; Carballa, M.; Noppe, H.; De Brabander, H.; Boon, N.; Verstraete, W. Influence of Manganese and Ammonium Oxidation on the Removal of 17 α -Ethinylestradiol (EE2). *Water Res.* **2009**, *43* (1), 77–86.

(65) Li, F.; Liu, C.; Liang, C.; Li, X.; Zhang, L. The Oxidative Degradation of 2-Mercaptobenzothiazole at the Interface of β -MnO₂ and Water. *J. Hazard. Mater.* **2008**, *154* (1–3), 1098–1105.

(66) Chowdhury, S.; Champagne, P.; McLellan, P. J. Models for Predicting Disinfection Byproduct (DBP) Formation in Drinking Waters: A Chronological Review. *Sci. Total Environ.* **2009**, *407*, 4189–4206.

(67) US Environmental Protection Agency *Comprehensive Disinfectants and Disinfection Byproducts Rules (Stage 1 and Stage 2): Quick Reference Guide*; EPA 816-F-10–080; US EPA, Office of Water: Washington, DC, 2010.

(68) Edwards, E. C.; Harter, T.; Fogg, G. E.; Washburn, B.; Hamad, H. Assessing the Effectiveness of Drywells as Tools for Stormwater Management and Aquifer Recharge and Their Groundwater Contamination Potential. *J. Hydrol.* **2016**, *539*, 539–553.

(69) Manceau, A.; Lanson, M.; Geoffroy, N. Natural Speciation of Ni, Zn, Ba, and As in Ferromanganese Coatings on Quartz Using X-Ray Fluorescence, Absorption, and Diffraction. *Geochim. Cosmochim. Acta* **2007**, *71* (1), 95–128.

(70) Post, J. E. Manganese Oxide Minerals: Crystal Structures and Economic and Environmental Significance. *Proc. Natl. Acad. Sci. U. S. A.* **1999**, *96* (7), 3447–3454.

(71) Alidina, M.; Li, D.; Drewes, J. E. Investigating the Role for Adaptation of the Microbial Community to Transform Trace Organic Chemicals during Managed Aquifer Recharge. *Water Res.* **2014**, *56*, 172–180.

(72) Rudder, J. d.; Wiele, T. V. de; Dhooze, W.; Comhaire, F.; Verstraete, W. Advanced Water Treatment with Manganese Oxide for the Removal of 17 α -Ethinylestradiol (EE2). *Water Res.* **2004**, *38* (1), 184–192.

(73) Knocke, W. R.; Occiano, S. C.; Hungate, R. Removal of Soluble Manganese by Oxide-Coated Filter Media: Sorption Rate and Removal Mechanism Issues. *J. - Am. Water Works Assoc.* **1991**, *83* (8), 64–69.

(74) Goren, O.; Lazar, B.; Burg, A.; Gavrieli, I. Mobilization and Retardation of Reduced Manganese in Sandy Aquifers: Column Experiments, Modeling and Implications. *Geochim. Cosmochim. Acta* **2012**, *96*, 259–271.

(75) McKenzie, R. The Adsorption of Lead and Other Heavy Metals on Oxides of Manganese and Iron. *Aust. J. Soil Res.* **1980**, *18* (1), 61.